Check for updates

Ecohydrology

WILEY

RESEARCH ARTICLE OPEN ACCESS

Continuous Stem Water Potential Measurements With Microtensiometry Reveal Species Identity and Soil Matric Potential Control of Stem Water Potential in Temperate Forests

Ruth-Kristina Magh[1,2] | Sharath Shyamappa Paligi[3] | Phillip Papastefanou[4] | Anne Klosterhalfen[5] | Christian Ammer[6] | Matthias Beyer[7] | Maren Dubbert[8] | Simon Haberstroh[9] | Clara Rohde[8] | Christiane Werner[9] | Anke Hildebrandt[1,2,10]

[1]Terrestrial Ecohydrology, Friedrich-Schiller-University, Jena, Germany | [2]German Center for Integrative Biodiversity Research (iDiv) Halle-Jena-Leipzig, Leipzig, Germany | [3]Plant Ecology and Ecosystems Research, Albrecht von Haller Institute for Plant Sciences, University of Goettingen, Goettingen, Germany | [4]Max-Planck Institute for Biogeochemistry, Jena, Germany | [5]Bioclimatology, University of Göttingen, Göttingen, Germany | [6]Silviculture and Forest Ecology of the temperate Zones, University of Göttingen, Göttingen, Germany | [7]TU Braunschweig, Institute of Geoecology, Isodrones, Braunschweig, Germany | [8]Zentrum für Agrarlandschaftsforschung, RA 1 Landscape Processes, Ecophysiology of Water and Matter Cycling, Müncheberg, Germany | [9]Ecosystem Physiology, UNR, University of Freiburg, Freiburg, Germany | [10]Helmholtz Centre for Environmental Research - UFZ, Terrestrial Ecohydrology, Leipzig, Germany

Correspondence: Ruth-Kristina Magh (ruth.magh@posteo.net)

Received: 2 July 2025 | **Revised:** 2 February 2026 | **Accepted:** 6 March 2026

Keywords: environmental gradients | hydraulic status | microsensors | plant–soil interactions | tree hydraulics | water availability

ABSTRACT

Water potential gradients govern water fluxes, and plants respond with species-specific hydraulic traits that influence ecosystem function. While understanding these traits is key to predicting vegetation responses to climate change, traditional methods like the pressure chamber limit temporal resolution and continuity. Additionally, suitable methods for continuous monitoring remain limited. We addressed this gap by evaluating the potential of microtensiometers for continuous stem water potential (ψ_{stem}) monitoring in mature forest trees across three temperate sites. We collected ψ_{stem} data over the 2023–2024 vegetation periods from 21 microtensiometers installed in *Fagus sylvatica*, *Fraxinus excelsior* and *Carpinus betulus*, alongside high-frequency soil matric potential (ψ_{soil}) measurements and meteorological data. Microtensiometers provided realistic daily cycles and good agreement with pressure chamber-derived leaf water potential (ψ_{leaf}). Crucially, our results show that ψ_{soil}, next to species identity, is one dominant driver of stem water potential across sites. Diurnal patterns showed that ψ_{stem} is driven by shallow soil layers during the day, when strong transpirational pull creates more negative ψ_{stem}, enabling access to these drier upper soils. At night, when transpiration ceases and ψ_{stem} becomes less negative, deeper, wetter soil layers predominantly supply water, reflecting the physical constraints of water flow within the root zone. This soil control was consistent across all species and sites under moderately dry to normal conditions. We further show that ψ_{stem} data can support broader physiological analyses, including refining tree water deficit–water potential relations and highlighting spatial variability in root water uptake. Our findings indicate that horizontal and vertical ψ_{soil} heterogeneity must be accounted for to avoid oversimplified interpretations of plant water use. This study demonstrates that microtensiometers can provide continuous, nondestructive measurements of plant water status and, when carefully installed and continuously monitored, can reveal meaningful ecological patterns while also requiring attention to methodological constraints. Most notably, we show that species identity and soil moisture regulate stem water potential, underscoring the central role of soil–plant interactions in shaping forest water dynamics under changing climatic conditions.

This is an open access article under the terms of the Creative Commons Attribution License, which permits use, distribution and reproduction in any medium, provided the original work is properly cited.

© 2026 The Author(s). *Ecohydrology* published by John Wiley & Sons Ltd.

1 | Introduction

Gradients in water potential ($\Delta\psi$) drive water movement through a continuous hydrological system (Hillel 2003). In plants, differences in water potential drive water uptake from the soil through the xylem and out of the stomata, forming transpiration (Philip 1966). With sufficient soil moisture, xylem water potentials are only slightly negative, but they decrease strongly when soils dry out or the transpirational demand is high. This increases hydraulic resistance and results in even more negative xylem water potentials to maintain access to soil water (Mencuccini et al. 2019; Torres-Ruiz et al. 2024). Under extreme conditions, growing impediments to water flow along the soil–plant–atmosphere path elevate the risk of xylem embolism, ultimately leading to hydraulic failure (Choat et al. 2018; Sperry et al. 2002). Therefore, xylem water potential (ψ_{xylem}) is the essential indicator of plant water status (Bhaskar and Ackerly 2006; Brodersen et al. 2019; De Swaef et al. 2022).

The most commonly used and well-established approach to measure plant water potentials is the pressure chamber method (Buckley and Sack 2024; Scholander 1966). The so obtained water potential provides the most useful measure of plant water stress (Lösch 2003). However, it only allows for limited resolution in time and/or space due to its destructive and labour-intensive nature. Despite these constraints, the pressure chamber has contributed substantially to our understanding of plant hydraulics. For example, pressure–volume curves obtained using this method were instrumental in revealing the relationship between ψ_{leaf} and transpiration rates during soil drying (Cochard et al. 2002). Similarly, using the pressure chamber in combination with exuding sap, Henzler et al. (1999) demonstrated that root hydraulic conductivity varies between days.

Building on these insights, advances in sensor technology have enabled continuous measurements of xylem water potential, offering new opportunities to deepen the understanding of water fluxes through the soil–plant–atmosphere continuum (Novick et al. 2022). Continuous data allow for the quantification of water potential gradients within the plant—from the roots, through the stem, into the canopy—which, when combined with sap flow measurements, enables assessments of in situ hydraulic conductivity and flow resistance (Schenk et al. 2020). Furthermore, temporal evolution of ψ_{xylem} allows reassessment of long-standing concepts such as the isohydric-anisohydric framework of plant water use strategies, which has been questioned (e.g., Garcia-Forner et al. 2017; Hochberg et al. 2018; Paligi et al. 2024). Instead, alternative concepts could be proposed, for example, interpreting stomatal regulation as a plant–environment interaction rather than a strict plant trait (Volaire 2018). Guo et al. (2020) found that the same species were able to exhibit different strategies over the course of the vegetation period by monitoring continuously. However, their data consisted of only six replicas, probably because of the high price of the psychrometers used.

Few methods currently allow for continuous observation of plant water potential (ψ_{plant}). Among these methods, psychrometry gained recent attention, though established for several decades, and is based on the psychrometric principle (Ehlig 1962; Richards and Ogata 1958; Savage et al. 1983). Psychrometers measure plant water potential following the thermodynamic relationship between water potential and the vapour pressure of water, whereby differences in vapour pressure between the plant tissue and the sensor are used to infer water potential (Dixon and Tyree 1984). This principle provides a high sensitivity across a wide range of water potentials and overcomes spatial and temporal limitations of the pressure chamber method by enabling real-time tracking of dynamic processes (e.g., Guo et al. 2020). However, psychrometers remain technically complex as they require careful protection from thermal gradients and require frequent accurate calibration. In addition, the costly nature of these sensors makes large-scale installation and long-term data collection more challenging under field conditions. More recently, microtensiometers have emerged as a direct and promising method for measuring plant water potential following the principle of liquid phase tension (Blanco and Kalcsits 2021; Lakso et al. 2022; Pagay 2022; Pagay et al. 2014). These sensors are relatively easy to instal, require minimal maintenance and can operate continuously, providing high temporal and spatial resolution of ψ_{plant}. Compared with psychrometers, microtensiometers are more affordable and facilitate broader deployment under field conditions. However, accurate measurements depend on establishing good hydraulic contact between the sensor and the xylem, and microtensiometers may cavitate under very dry conditions (manufacturer recommended lower limit of −3.5 MPa) or freezing temperatures (FloraPulse Co., Davis, CA, USA). Moreover, microtensiometers require a certain branch diameter (depending on specification), where psychrometry technique retain an advantage, as they can be used to measure both leaf and woody xylem water potential (Campbell and Campbell 1974). Consequently, the choice of the method should be guided by the specific research question. Additionally, several indirect alternatives have emerged, such as high resolution dendrometry, which in combination with periodic direct measurements by the pressure chamber method, provides continuous data of ψ_{plant} (Gleason et al. 2024). Another indirect option to assess ψ_{plant} are optical dendrometers to monitor tissue shrinkage as a ψ_{stem} proxy (Bourbia et al. 2021, 2022; Bourbia and Brodribb 2023).

These technical advances allow for deeper insights along several current lines of research. Beyond revisiting established concepts, continuous water potential measurements also open valuable new applications in plant hydraulics research. First, the plant hydraulics community uses hydraulic variables such as tree water deficit (TWD) and ψ_{leaf} (Dietrich et al. 2018; Ziegler et al. 2024) or sap flow (Donfack et al. 2026) to link environmental stressors to plant physiological behaviour during soil drying or high VPD. The link between TWD and continuous ψ_{plant} seems particularly promising to further unravel plant responses to drying soils.

Second, water potential measurements could support the investigation of factors limiting root water uptake (RWU), which sheds light on both plant physiological controls (Epila et al. 2017) and soil-related factors (Doussan et al. 2006). Plants regulate water loss along a fine-tuned interplay between supply and demand along the soil–plant–atmosphere continuum via RWU, transport and release, where stomatal conductance is

19360592, 2026, 3, Downloaded from https://onlinelibrary.wiley.com/doi/10.1002/eco.70197 by MPI 322 Chemical Ecology, Wiley Online Library on [30/03/2026]. See the Terms and Conditions (https://onlinelibrary.wiley.com/terms-and-conditions) on Wiley Online Library for rules of use; OA articles are governed by the applicable Creative Commons License

controlling transpirational losses (Buckley 2005; Meinzer 1993), while soil hydraulic properties and root–soil contact determine water availability (Doussan et al. 2006; Javaux et al. 2008). To answer the question to what extent soil or atmosphere shapes ψ_{plant}, continuous measurements could provide insights into the location of RWU, enhancing the methods portfolio.

Third, while isotopic approaches remain widely used for RWU studies (Dawson 1993; Evaristo et al. 2017), they often assume uniform ψ_{soil}, neglecting spatial heterogeneity within the rooting zone (but see Ogle et al. 2004; De Deurwaerder et al. 2020). By continuously monitoring ψ_{stem} alongside ψ_{soil} at several points within the same rooting zone, we could provide a direct assessment of whether specific soil layers are hydraulically accessible to plants. This approach offers an improved understanding of RWU patterns by incorporating spatial heterogeneity in soil moisture, which has often been ignored in previous studies.

Based on these considerations, we hypothesized that microtensiometers can reliably capture ψ_{stem} dynamics in temperate tree species and offer a meaningful link to traditional pressure chamber measurements of ψ_{leaf}. Furthermore, we expected that ψ_{stem} reflects environmental forcing across different sites and species, and that its continuous observation provides insight into both short-term atmospheric drivers and deeper soil-root water interactions. Finally, we hypothesized that ψ_{stem} can be used as a proxy to detect shifts in RWU patterns and water stress responses, with a clear relevance for linking hydraulic status to TWD.

We evaluated the field performance of the microtensiometer (FloraPulse Co., Davis, CA, USA) by comparing continuous ψ_{stem} measurements with periodic ψ_{leaf} values obtained using the pressure chamber method. This comparison was conducted at two different sites (ZALF and Hartheim) in two temperate tree species—*Fagus sylvatica* (European beech) and *Carpinus betulus* (European hornbeam)—across different times of the day and stages of the growing season. Because the application of novel sensors often comes with practical challenges, we also document recurring technical issues and the workarounds developed during field deployment.

We further analysed continuous ψ_{stem} time series across three sites, in three tree species: beech, hornbeam and common ash (*Fraxinus excelsior)* and determined its primary drivers from soil, plant and atmospheric perspectives. Using boosted regression trees, we identified the most influential variables driving ψ_{stem} variability during the climatologically average summer of 2023 in Germany (see SPEI in Figure S4).

We conclude by showcasing potential applications for this novel approach to monitoring ψ_{stem} in situ by assessing the relation between ψ_{stem} and TWD and exploring estimates of RWU locations.

2 | Material and Methods

For this study, data were collected at three sites, harbouring different species and at varying time resolutions. While we aimed to harmonize the datasets, not all sites provided all measurements. Therefore, we first provide a description of the study sites, followed by an overview of the sensor setup (i.e., stem water potential, soil matric potential, soil moisture and environmental data). Finally, we provide a description of quality control, data flagging and filtering procedures and statistical analyses, which were standardized across sites. For clarity, Table 1 summarizes the data available at each site and the corresponding analyses conducted.

2.1 | ZALF Field Site

One performance assessment for the microtensiometer was conducted at a study site on the grounds of the Leibniz Centre for Agricultural Landscape Research (ZALF) in Müncheberg,

TABLE 1 | Data description and availability for each investigated site.

	Data					
Site	Continuous ψ_{soil} and ψ_{stem}	Environmental data	Pressure chamber $\psi_{leaf/branch}$	Used for assessment of sensor utility	Used for boosted regression analysis	Used for TWD/potential and RWU estimates
Hartheim	Yes, at 20-min resolution	Yes, ICOS (De-Har; Christen, Baab, et al. 2024)	Yes, 5 times per season	Yes	Yes	No
Hainich	Yes, at 10-min resolution	Yes, ICOS (De-Hai; Knohl et al. 2024)	No	No	Yes	Yes
Apelern	Yes, at 30-min resolution	Yes, Atmos-41 station (2-m height), DWD stations nearby: 294, 4112	No	No	Yes	No
ZALF	No, only ψ_{stem} over a 3-day course	Yes, DWD weather station 03376	Yes, every 1 h for 3 days	Yes	No	No

19360592, 2026, 3, Downloaded from https://onlinelibrary.wiley.com/doi/10.1002/eco.70197 by MPI 322 Chemical Ecology, Wiley Online Library on [30/03/2026]. See the Terms and Conditions (https://onlinelibrary.wiley.com/terms-and-conditions) on Wiley Online Library for rules of use; OA articles are governed by the applicable Creative Commons License

50 km east of Berlin, Germany (52°30′58″ N, 14°07′03″ E). The site consists of a small, forested area situated between research buildings, greenhouses and field experimental plots. The average annual temperature is 9.5°C, with an average annual precipitation of 535 mm (DWD, February 28, 2024, Station Number: 03376, long-term average from 1991 to 2020). The underlying geological substrate consists of glacial sands on which podzolic brown earths and, to a lesser extent, brown earths and podzol-brown earths have formed. However, since this is a site directly adjacent to the ZALF's main campus, construction activities have most likely resulted in strong disturbance of previously established soil horizons. Two trees were used for investigation—a beech and a hornbeam.

2.1.1 | Installation and Sampling

Microtensiometers (analogue probes) were installed roughly at breast height into a beech and a hornbeam individual following the protocol provided by the manufacturer (FloraPulse: Resources 2025).

Briefly, the sleeve holding the sensor was tightly hammered into the tree stem until it did not penetrate further. We worked without prior bark removal, since both beech and hornbeam are thin-barked species. We drilled a hole into the stem underneath the sleeve, drilling roughly 2 mm at a time with subsequent removal of wood shavings using the manufacturer-provided drill bit. We stopped drilling once the xylem was exposed, after which the surface was examined regarding being flat and without discolouration. We used a spatula to scrape off remaining wood debris. The sleeve was then filled with mating compound (a clay-water mixture provided by the manufacturer) and the sensor was placed into the hole and fixed in place with a spring and a cap, which were part of the installation package. Excess mating compound was removed using tissues and the sleeve was greased to seal.

For all other installations of microtensiometers (see Sections 2.2.1, 2.3.1 and 2.4.1), this same protocol was followed unless specified otherwise.

Here, ψ_{stem} was logged in units of bar at 5-min interval on a CR1000 data logger (Campbell Scientific Logan, UT, USA).

Every hour between 08:00 and 17:00 for the course of the days from 11/09 through 13/09, small branches were cut from the tree crown at roughly 10- to 13-m height using pole cutters. The cut surface was smoothed with a razor blade before measurement. We did not cover the leaves in tin foil before measuring. The water potential was then measured using a scholander pressure chamber (Soilmoisture Equipment Corp., Santa Barbara CA, USA, Model 3115).

2.2 | Hainich Field Site

The field site lies within the Hainich National Park in Thuringia, Germany (51°04′46″ N, 10°27′08″ E, 440 m above sea level). The average annual temperature is 9°C, and the average annual precipitation is 694 mm (DWD, Station Number: 7368, 30-year long-term average: 1991 to 2020). The local soils consist of silty-clayey Cambisols, 0.5–0.7 m deep, overlying Triassic limestone and Pleistocene loess deposits (Mund et al. 2020). Before the establishment of Hainich National Park in 1997, the Hainich forest was a military restricted area for several decades, allowing nature to develop undisturbed in inaccessible parts of the forest (Knohl et al. 2003; p.comm. Nationalpark Hainich, 28 February 2023). The tree population consists of European beech (64%), common ash (28%), sycamore maple (*Acer pseudoplatanus*, 7%) and other deciduous tree species (Tamrakar et al. 2018). Tree density is 325 trees per hectare (stem diameter > 7 cm) (as of 2011; Mund et al. 2020). The forest stand is classified as an unmanaged, uneven-aged mixed deciduous forest. The trees in the study area reach maximum heights of 30 to 38 m and are up to 270 years old (Knohl et al. 2003). In spring, the herb layer is dominated by wild garlic (*Allium ursinum*) and wood anemone (*Anemone nemorosa*). The study site is located within the main footprint of an Eddy Covariance tower of the ICOS network (DE-Hai, associated site). At a height of 42–44.5 m, continuous measurements of meteorological variables and of carbon dioxide, water vapour and energy fluxes are conducted using the eddy covariance technique (Knohl et al. 2003; Tamrakar et al. 2018).

2.2.1 | Installations and Sampling

Microtensiometers (both analogue (2023) and digital (2024) probes) were installed in individuals of beech and ash ($n = 4$ individuals per species with each 1 sensor) in the early growing season of 2023 following the protocol described in Section 2.1.1. Data retrieval started in mid-June 2023.

In 2024, we installed the microtensiometers in 4 tree individuals (two beech and two ash individuals, partly the same trees as the previous year). We installed three sensors per tree: one in a horizontal root running up to the main stem, one in the main stem at breast height, and one in the main stem in the tree crown (~27 m height). We followed the updated protocol (see Magh and Paligi 2024) and were able to collect data from late May until the beginning of November 2024.

Tree girth increments were measured using high-resolution dendrometers (DRS 26; EMS Brno, Czech Republic) installed at breast height. Prior to installation, the bark surface at the designated height was cleaned with a stiff brush to ensure a secure attachment of the stainless-steel fixing band (12 × 0.2 mm). The dendrometers operated with an accuracy of 0.1 mm, a resolution of 1 µm, and functioned within a temperature range of 40 to 60°C (EMS Brno 2022). Each device recorded two parameters: changes in tree circumference [mm] and operating temperature (°C). The circumference measurements were automatically adjusted to account for potential temperature-induced effects on the system. For this study, we analysed data collected from ash tree 7 (Figure 1) during the 2024 growing season.

In 2023, we installed 22 soil sensors within the rooting zones of three tree individuals (one beech, two ashes): soil matric potential (MPS6, UMS corresponding to Teros21, Meter, Munich, Germany) and volumetric soil water content (SMT100, Truebner, Neustadt, Germany) in the same soil pits (approximately 30 cm

19360592, 2026, 3, Downloaded from https://onlinelibrary.wiley.com/doi/10.1002/eco.70197 by MPI 322 Chemical Ecology, Wiley Online Library on [30/03/2026]. See the Terms and Conditions (https://onlinelibrary.wiley.com/terms-and-conditions) on Wiley Online Library for rules of use; OA articles are governed by the applicable Creative Commons License

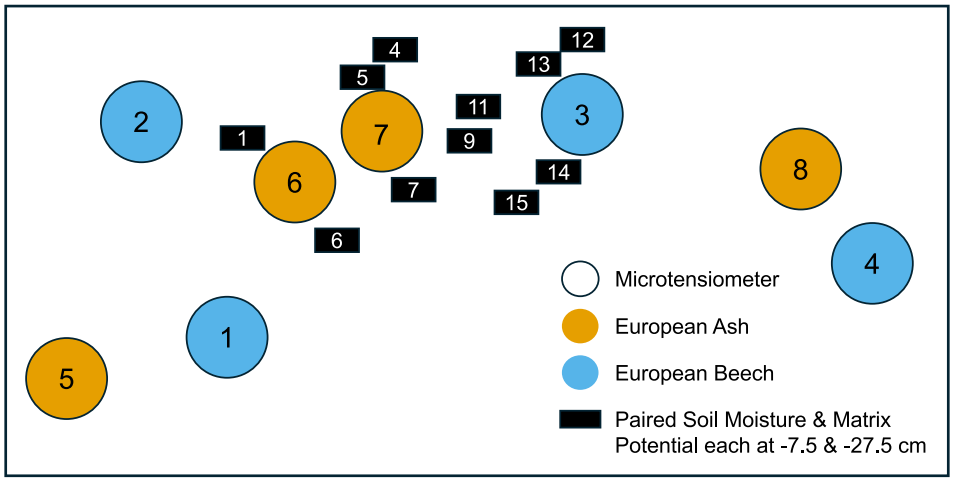


FIGURE 1 | Overview over the spatial distribution of paired soil moisture and matrix potential sensors in the Hainich plot.

from each other) at two depths (upper sensors at 7.5 and lower sensors at 27.5-cm soil depth). Installations were completed in May 2023 and soil pits were refilled after installation. A spatial overview of the installation is given in Figure 1. Distances from the individual tree to the respective sensor pair are given in Table S1.

Soil matrix potential (hPa) and temperature (°C) were collected from the MPS6 sensors on a CR1000 logger (Campbell Scientific Logan, UT, USA) at 10-min resolution, and soil moisture and temperature were logged at the same interval on a TrueLog100 (Truebner, Neustadt, Germany) logger.

2.3 | Apelern Site

The small catchment (~1 km^2) is in Apelern, located in the Weserbergland near the city of Hannover (52°16′52″ N, 9°18′38″ E, 140 m above sea level). Average annual temperature is 9.8°C and the average annual precipitation 576 mm (DWD station 15,939). Over a haplic Luvisol with multiple continuous impeccable layers lies a near-natural mixed forest consisting mainly of beech, oak (*Quercus* spp.), hornbeam, ash and little-leaf linden (*Tillia* spp.). The hillslope drains into a small river with a seasonally highly variable water table. Three different plots were chosen along the hillslope: top hill (plot 1), slope (plot 2), valley (plot 3) where three microtensiometers per plot were installed, respectively in an ash (diameter at breast height (DBH) 34.73 ± 4.65 cm), beech (DBH 35.5 ± 6.9 cm), and hornbeam (DBH 18.7 ± 0.8 cm) individual. The height of the forest is between 27 and 35 m.

2.3.1 | Installation and Sampling

Microtensiometers (analogue probes) were installed in the trunk of three ash, beech, hornbeam trees at breast height in April 2023, elongated and connected to a CR1000 datalogger (Campbell Scientific Logan, UT, USA) in late June 2023 with 30 min measuring interval. Sensors were shielded with the provided reflective aluminium foil to minimize thermal influences. No further maintenance or reinstallation was done until uninstallation in November 2023.

At each of the plots, soil matric potential sensors (Metergroup, TEROS-21) were installed by pushing them into the side walls of each excavated soil pit, in the upper soil (5–10 cm) and depending on how deep installation could be realized (maximum installation depths: plot 1–3.5 m; plot 2–2.5 m; plot 3–1.8 m). The soil pit was closed thereafter. Measurements were taken every 30 min using Campbell CR1000 data loggers (Campbell Scientific Logan, UT, USA).

Weather data (rainfall, wind speed & direction, solar radiation, relative humidity, temperature) were recorded with an Atmos-41 (Metergroup) all-in-one system at 2 m height. Inside the forest, an additional set of radiation, temperature and relative humidity sensors were installed to monitor within-stand conditions.

2.4 | Hartheim Site

The field site in Hartheim is located in the Upper Rhine valley close to the city of Freiburg, Germany (47°56 N, 7°36 E, 201 m above sea level). The average air temperature is 10.6°C (1991–2020) with an annual precipitation sum of 646 mm (1991–2020) (Christen, Imbery, et al. 2024). The Hartheim forest research site is ICOS associated (DE-Har) and allows access to the tree canopy by two towers (18 m and 30 m). Located on a former floodplain of the Rhine-valley, carbonate-rich, two-layer Haplic Regosols have developed (Goffin et al. 2014). In 1963 a Scots Pine (*Pinus sylvestris* L.) forest has been planted with a size of 0.7 ha (Holst et al. 2008), however, > 60% of Scots Pine trees had died by 2023 due to the impact of the severe 2018 drought (Haberstroh et al. 2022). In the canopy openings, a diverse understory of several deciduous tree species has developed, including hornbeam, beech or lime species (*Tilia* spp.). Three hornbeam trees were chosen for microtensiometers installation due to their proximity to the tower and canopy accessibility (Haberstroh et al. 2025). Trees had a height of 10.8 ± 0.3 m (±1 SE) and diameter at breast height of 17.1 ± 0.8 cm.

19360592, 2026, 3, Downloaded from https://onlinelibrary.wiley.com/doi/10.1002/eco.70197 by MPI 322 Chemical Ecology, Wiley Online Library on [30/03/2026]. See the Terms and Conditions (https://onlinelibrary.wiley.com/terms-and-conditions) on Wiley Online Library for rules of use; OA articles are governed by the applicable Creative Commons License

2.4.1 | Installation and Sampling

Microtensiometers (analogue probes) were installed in the trunk of three hornbeam trees approximately 1 m above ground as described in Section 2.1.1 and connected to a CR1000 datalogger (Campbell Scientific Logan, UT, USA) in May 2023. The sensors were excited and measured every 20 min. Before installation, sensor cables were extended up to a length of 15 m with a shielded PVC control cable (for more details see Haberstroh et al. (2025)). Branch water potential was measured with a Scholander-type pressure chamber (1505D, PMS Instrument, USA) at 5 days between May and September 2023. Pre-dawn measurements were conducted between 4 and 6 AM (CEST); midday water potential was measured between 1 and 3 pm (CEST) on sunlit branches 8–10 m above ground. Leaves were not covered or bagged.

Soil water potential sensors (MPS-6, UMS, Munich, Germany) were installed at three depths (0.10, 0.25 and 0.50 m) close (within 6-m distance) to the measured trees in June 2023 and measured every 20 min on a data logger (ECH2O Em50, Decagon Devices, USA).

2.5 | Data Filtering and Correcting

Microtensiometer data from all sites were filtered to remove unrealistic values (> −6 MPa and < 0.05 MPa). The sensor provider specifies a guaranteed measurement range of 0 to −3.5 MPa, with an accuracy of 0.01 MPa, although measurements at lower water potentials have been reported (Lakso et al. 2022). We therefore extended the accepted range beyond the guaranteed specifications, as we found no evidence of systematic sensor failure within this range; however, we note that we did not independently validate sensor accuracy at these more negative water potentials.

Soil matric potential data at all three field sites were collected with the same sensor type (MPS6/Teros21; see above), and data were subsequently temperature corrected following the approach of Walthert and Schleppi (2018), using Equation (1):

$$\Delta pF = \left(11.54 * \Delta T + 0.2206 * \Delta T^2\right) * \exp\left(-\frac{29.50}{pF + 0.8426}\right) \quad (1)$$

where $pF = \log(-\psi)$, ΔT is the temperature read by the sensor with regard to the reference temperature (22°C).

Atmospheric water potential (ψ_{atmo}) was calculated using meteorological data from the respective site (either from the eddy covariance tower—Hainich (Knohl et al. 2024) and Hartheim (Christen, Baab, et al. 2024)—or the station installed onsite [Apelern]), using the following equation:

$$\psi_{atmo} = \frac{RT}{V_w} \ln\left(\frac{rH}{100}\right) \quad (2)$$

where ψ_{atmo} represents the atmospheric water potential (Pa), R is the gas constant (8.314 j $mol^{-1} K^{-1}$), T the air temperature in K, V_w the molar volume of water (for simplicity set to 18 $m^3 mol^{-1}$), and rH is the relative humidity.

2.6 | Statistical Analyses

Most statistical analyses were conducted using R (R Core Team 2023). The data were then visualized using the *tidyverse* package (Wickham et al. 2019).

Data analyses for Section 2.6.3 were conducted in Python version 3.11.8 (Van Rossum and Drake 2009) using the packages *scikit-learn* (Pedregosa et al. 2011), *numpy* (Harris et al. 2020), *pandas* (McKinney 2010) and *matplotlib* (Hunter 2007).

2.6.1 | Relationship Between High-Resolution Leaf- and Continuous ψ_{stem} at ZALF Field Site

To assess the relationship between ψ_{stem} (measured with the microtensiometer) and $\psi_{leaf/branch}$ (measured by the pressure chamber), we employed generalized additive models (GAMs) using the *mgcv* package in R (Wood 2011). Given the observed nonlinear relationship, GAMs were chosen for their flexibility in capturing smooth, data-driven trends without imposing a predefined functional form. Separate GAMs were fitted for each species to account for potential interspecific differences. The models were specified as:

$$\psi_{stem,i} = s\left(\psi_{leaf,i}\right) + \epsilon_i \quad (3)$$

where ψ_{stem} represents the stem water potential for species i, ψ_{leaf} the leaf water potential for species i, and s ($\psi_{leaf,i}$) is a species-specific smooth function modelled using cubic regression splines. The residual error term ε_i accounts for unexplained variation. Smoothing parameters were selected using restricted maximum likelihood (REML) to prevent overfitting. Model performance was assessed using the coefficient of determination (R^2), which was computed separately for each species.

2.6.2 | Relationship Between Leaf and ψ_{stem} Over the Seasonal Course at the Hartheim Field Site

To assess the relationship between ψ_{stem} (measured with the microtensiometer) and $\psi_{leaf/branch}$ (measured by the pressure chamber) over the seasonal course of 2023 at the Hartheim site, we used linear models, grouping each measurement time point ($n = 3$ individual hornbeam trees measured at the same time). The relationship between pre-dawn and midday ψ was then assessed per measurement day.

2.6.3 | Drivers of ψ_{stem} at All Three Field Sites Using Random Forest Regression Analysis

To estimate the impacts of environmental factors on stem water potential, we performed a random forest regression analysis. We selected the following nine feature variables as predictors: Relative humidity, air temperature, atmospheric water potential, the Standardized Precipitation Evapotranspiration Index (SPEI) for 3 and 12 months, respectively, the soil matric

19360592, 2026, 3, Downloaded from https://onlinelibrary.wiley.com/doi/10.1002/eco.70197 by MPI 322 Chemical Ecology, Wiley Online Library on [30/03/2026]. See the Terms and Conditions (https://onlinelibrary.wiley.com/terms-and-conditions) on Wiley Online Library for rules of use; OA articles are governed by the applicable Creative Commons License

potential of uppermost, middle, and lowest soil layers, and an integer reflecting the three species across the sites. As target variable, we chose the average ψ_{stem} per species per site. Before model training and testing, we subdivided the dataset per hour and trained 24 random forest models, one per hour. We chose this subdivision to prevent the model from focusing on the diurnal cycle in water potential, which closely follows temperature patterns or patterns in humidity. We further divided the dataset into 80% for training and 20% for testing and used R^2 as performance score.

2.6.4 | Calculation of TWD and Relation to Stem Water Potential

For the TWD calculations, we used band-dendrometer data from an ash individual at the Hainich site. Due to data availability and compatibility, we were able to use data from late May (DOY 149) through mid-September (DOY 254) 2024. The dendrometer was installed in the same tree (ash 7; see Figure 1) in which microtensiometers were installed in 2024 so that we had three sets of water potential data (horizontal root, stem at breast height and upper stem at ~27 m) available to compare to the dendrometer dataset.

We followed Dietrich et al. (2018), to calculate maximum daily shrinkage as a predictor for the stem water potential. Briefly, we created horizontal segments connecting each local maximum stem radius to the next maximum in time. These segments then represent the last maximum stem radius in the observed period. The difference between this line and the current daily minimum stem radius was defined as the TWD for the respective day. This method assumes growth occurs only when the stem radius surpasses the previous maximum. All TWD metrics quantify absolute stem water deficit, reaching zero when tissues are fully hydrated. To facilitate modelling, TWD and ψ_{stem} were normalized by dividing daily values by the highest species-specific TWD/the most negative water potential observed (relative TWD/ψ).

To relate the TWD to the measured potentials, we used the nls() of the R *stats* package to fit a logistic equation:

$$\mathrm{TWD}_{\mathrm{relative}} = \frac{L}{1 + e^{-k*(\varphi_{\mathrm{relative}} + x_0)}} \tag{4}$$

where L, k and x_0 are model coefficients: L is the asymptote value approaching $\mathrm{TWD}_{\mathrm{relative}}$, k is the steepness of the curve, and x_0 is the infliction point. Statistical significance of the model fit was assessed using the p value obtained from an F test, which evaluates whether the model explains significantly more variance than a null model. For nonlinear regression (nls), where p values are not directly provided, model significance was inferred from the reduction in residual sum of squares compared with a simpler model. We additionally calculated the coefficient of determination (R^2) using Equation (4):

$$R^2 = 1 - \frac{\mathrm{RSS}}{\mathrm{TSS}} \tag{5}$$

where RSS is the residual sum of squares (between observed and predicted values) and TSS is the total sum of squares (total variability in the data).

2.6.5 | Calculating Potential for RWU in the Rooting Zone

RWU from the soil is only possible if the water potential of the tree is lower than that of the soil surrounding its roots. To identify soil layers available for RWU we calculated the difference between ψ_{stem} (at DBH) and the soil matric potential per soil layer:

$$\Delta\psi = \psi_{\mathrm{stem}} - \psi_{\mathrm{soil}} \tag{6}$$

If the potential gradient ($\Delta\psi$) was negative, RWU from this part of the soil was considered possible; if it was positive, RWU was not possible.

2.7 | Common Problems and Solutions

A key challenge in this study was the installation of novel microtensiometers, as no prior experience existed with these sensors in temperate deciduous tree species. Several common issues arose across all field sites, such that the initial data readings were unreliable, requiring adjustments. We summarize an overview of problems and solutions below (a detailed installation and troubleshooting protocol, addressing these challenges and their solutions, is described in Magh and Paligi (2024)). The most frequent issues and their respective solutions included:

1. **Installation depth**: In ring-porous and thick-barked species, improper installation depth was a major source of error in ψ_{stem} measurements, resulting in little to no variability of readings. The problem occurred most frequently for microtensiometers in ash trees due to small sapwood depth and required reinstallation to ensure correct placement.
2. **Cable extensions**: Standard cable length for the Florapulse sensors was not sufficient to connect to data loggers in many locations. Extending the cables of analogue probes requires shielded cables or a digital converter to maintain signal integrity. The more expensive version with SDI-12 interface prevents this problem.
3. **Water intrusion**: Wounding response or rain events can flood the sensor installation site and can lead to prolonged zero readings. This issue was resolved through reinstallation. The rainwater intrusion can be prevented by applying a protective sealing cover using silicone and water intrusion through wounding response from the nearby bark can be avoided by creating a similar covering around the sensor.
4. **Deteriorating signal strength**: We repeatedly observed a trend of increasingly negative water potential readings over time, without corresponding environmental drivers (e.g., no soil dry-down or high atmospheric demand), likely related to poor hydraulic contact between the sensor and

19360592, 2026, 3, Downloaded from https://onlinelibrary.wiley.com/doi/10.1002/eco.70197 by MPI 322 Chemical Ecology, Wiley Online Library on [30/03/2026]. See the Terms and Conditions (https://onlinelibrary.wiley.com/terms-and-conditions) on Wiley Online Library for rules of use; OA articles are governed by the applicable Creative Commons License

the xylem. This could be caused by the gradual drying of the sensor interface due to a vapour pressure gradient between the xylem and the surrounding, drier atmosphere. As the mating compound dehydrates, the sensor loses the hydraulic contact with the xylem water, leading to erroneous readings. Regreasing or reinstalling the sensor typically restores proper function.

As seen above, the solution to most problems involved sensor *reinstallation*. Although this was initially not recommended by the manufacturer, a new manual (found here: https://florapulse.com/resources/ under User Manuals, last access 22.04.2025) includes information on measures to clean uninstalled sensors and a test for sensor functionality, suggesting that reinstallation is possible. Following those instructions, we have successfully reinstalled microtensiometers at Hainich and Hartheim (with losses of ~10% after the first season).

3 | Results

3.1 | Assessment of Microtensiometer Performance by Comparing With Pressure Chamber Measurements

3.1.1 | Hourly ψ_{leaf} Versus Continuous ψ_{stem} at ZALF Field Site

One assessment of performance for the microtensiometer was conducted by comparing hourly measured leaf water potentials obtained by a pressure chamber with continuous measurements of stem water potentials using a microtensiometer over a 3-day course between 08:00 and 16:30 each day.

The data from the beech and hornbeam tree show a general offset from the 1:1 line which is expected from the hydrostatic gradient (Figure 2). The GAM between the leaf and ψ_{stem} indicates good agreement (beech: deviance explained = 78% and hornbeam: deviance explained = 90%), when accounting for the increase in potential difference toward midday between ψ_{stem} and $\psi_{leaf/branch}$. This increase is observable for both species and peaks between 11:00 and 12:00, after which it decreases again toward the late afternoon (Figure 2, Table S2).

3.1.2 | Seasonal Resolution ψ_{leaf} Versus Continuous ψ_{stem} at Hartheim Field Site

The second assessment of performance was conducted at the Hartheim field site, Figure 3 shows ψ_{leaf} and ψ_{stem} measured at the Hartheim site, of which ψ_{leaf} was measured pre-dawn and midday on the same day at five occasions in 2023. The linear regressions indicate agreement between pressure chamber measured ψ_{leaf} and microtensiometer measured ψ_{stem} ranging from $R^2 = 0.26$ to $R^2 = 0.88$ (Figure 3). The slopes of these regressions indicate that the relationship between ψ_{leaf} and ψ_{stem} changes with the measurement day, depending on the changes in ψ_{soil} over the season.

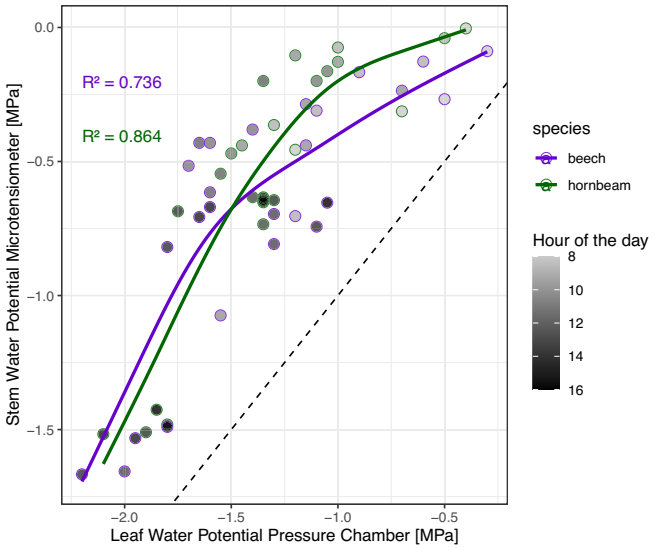


FIGURE 2 | Hourly ψ_{leaf} (*x*-axis) and ψ_{stem} (*y*-axis) measured on a beech (purple circles) and a hornbeam (green circles) over a 3-day course each between 08:00 and 16:30. The GAM fits are calculated by species (beech = purple, hornbeam = green) for the entire timeline (i.e., 3 days). The hour of the day is indicated by circle filling in shades from grey (early in the day) to black (last measurement in the late afternoon).

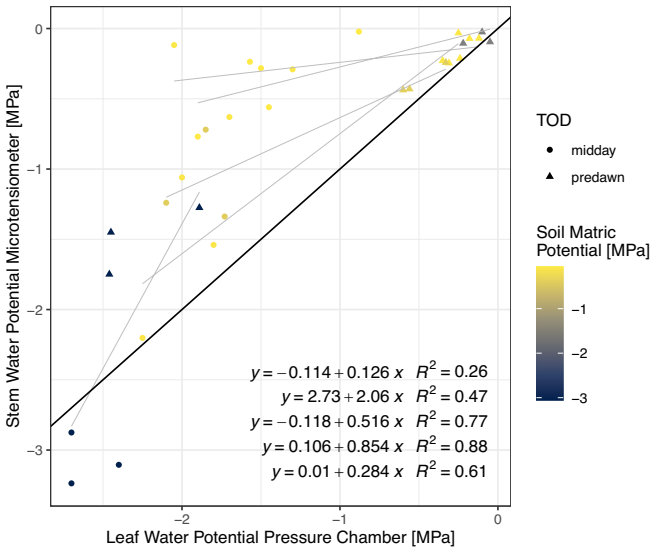


FIGURE 3 | ψ_{leaf} and ψ_{stem} measured predawn and midday on three hornbeam trees on different dates in the summer of 2023 using the pressure chamber and the microtensiometers. Colour coding indicates soil matric potential measured in 10-cm soil depth. Shape indicates predawn or midday measurements, and linear models represent the fits between pre-dawn and midday for five dates and for the three individuals ($n = 3$).

3.2 | Environmental Factors Influencing Diurnal Changes in Stem Water Potentials

The continuous ψ_{stem} data, measured in 2023, were categorized by species and aggregated by site; daily courses are plotted in Figure 4. Average diurnal patterns in ψ_{stem} were different between the three different species (Figure 4). Beech showed the highest ψ_{stem} and lowest diurnal variability (difference between

19360592, 2026, 3, Downloaded from https://onlinelibrary.wiley.com/doi/10.1002/eco.70197 by MPI 322 Chemical Ecology, Wiley Online Library on [30/03/2026]. See the Terms and Conditions (https://onlinelibrary.wiley.com/terms-and-conditions) on Wiley Online Library for rules of use; OA articles are governed by the applicable Creative Commons License

predawn and midday water potentials). Hornbeam had the overall greatest diurnal variability (predawn: highest water potential, midday: lowest water potential); also, the individual and site variability was greatest for midday water potential. Ash had the overall lowest water potentials at predawn and the overall largest variability between individuals and sites. The largest species differences in ψ_{stem} occurred in the night (between ash and beech/hornbeam) and during the late afternoon (between beech and ash/hornbeam; Figure 4).

Using random forests regression, we predicted ψ_{stem} well (R^2 above 0.87 of the test dataset) between 08:00 and 20:00, while model performance before and after that time was low (Figure S2).

Throughout the day the species ID (Figure 5a) and ψ_{soil} (Figure 5b, SHAP values in Figure S3) were the most important predictors of ψ_{stem} while the atmospheric drivers were of minor importance (Figure 5a). For ψ_{stem} the most influential driver was species ID, especially during the early morning (0.9; peaking at 08:00), then the importance decreases until reaching the lowest value of 0.6 in the later afternoon (between 16:00 and 18:00), after which it increases again (Figure 5a).

ψ_{soil} of the lower layer was mostly influencing ψ_{stem} in the early morning (peaking at 10:00, SHAP values in Figure S3a) and the evening (after 18:00), while the upmost soil layer was more important between 12:00 and 18:00 (Figure 5b, SHAP values in Figure S3b). Among the atmospheric predictors, temperature showed some importance during the day (peak at 18:00 with a feature importance of ~0.4), while the atmospheric water potential and relative humidity had almost no explanatory power (Figure 5a).

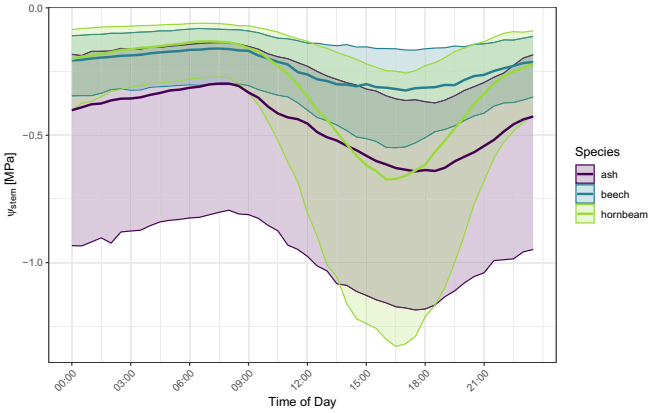


FIGURE 4 | Median (bold line) and quartiles (shaded area) of hourly ψ_{stem} of the three investigated tree species between early July and end of September for all sites. The colours depict the species, purple = ash, blue = beech, green = hornbeam.

3.3 | New Possibilities in Action

To highlight the potential of this newly available microtensiometer, here we show practical examples of how the measurements contributed insights to plant water relations using the observations from the Hainich dataset in 2024.

3.3.1 | Relation Between TWD and Stem Water Potential

We modified the approach of Dietrich et al. (2018), who predicted the water status of the canopy using TWD monitored by point dendrometers. Our aim was to test the relationship between TWD and tree water potential monitored by microtensiometers in the root, stem at breast height and stem at approximately 27 m height in the same tree (Figure 6, panels A, B, and C).

The relative TWD of the tree through the vegetation period of 2024 was related to ψ_{stem} in all three tree compartments (i.e., crown ($R^2 = 0.81$), stem ($R^2 = 0.87$), and root ($R^2 = 0.97$)),

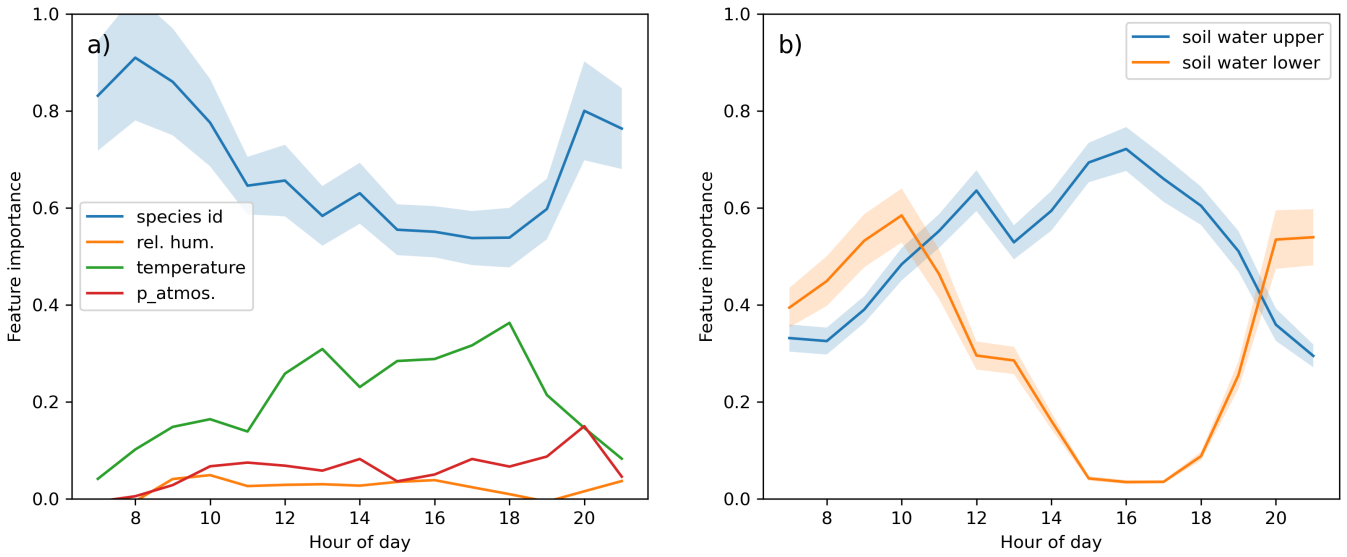


FIGURE 5 | Feature importance based on R^2 of (a) species (blue, includes beech, hornbeam and ash), air temperature (green), relative humidity (orange) and water potential of the atmosphere (red) and (b) the upper (blue) and lower (orange) ψ_{soil}, on the hourly prediction of ψ_{stem} across all sites (Hartheim, Hainich, Apelern) in 2023. Shaded areas behind the mean indicate one unit of standard deviation in feature importance.

19360592, 2026, 3, Downloaded from https://onlinelibrary.wiley.com/doi/10.1002/eco.70197 by MPI 322 Chemical Ecology, Wiley Online Library on [30/03/2026]. See the Terms and Conditions (https://onlinelibrary.wiley.com/terms-and-conditions) on Wiley Online Library for rules of use; OA articles are governed by the applicable Creative Commons License

and the model parameter estimates were highly significant ($p < 0.001$) with small residual errors. TWD and midday water potentials increased with progressing soil drying as indicated by colour in Figure 6. Short dry-down periods of the soil happened even in the normal to wet year 2024 (see SPEI Indices for the Hainich site in 2024 in Figure S1).

3.3.2 | Physical Constraints for Water Uptake Along the Depths Profile

The calculated gradient in water potential ($\Delta\psi$ in MPa/MPa) between the ψ_{stem} and ψ_{soil} at the Hainich site is presented in Figure 7. The negative gradients indicate that water uptake

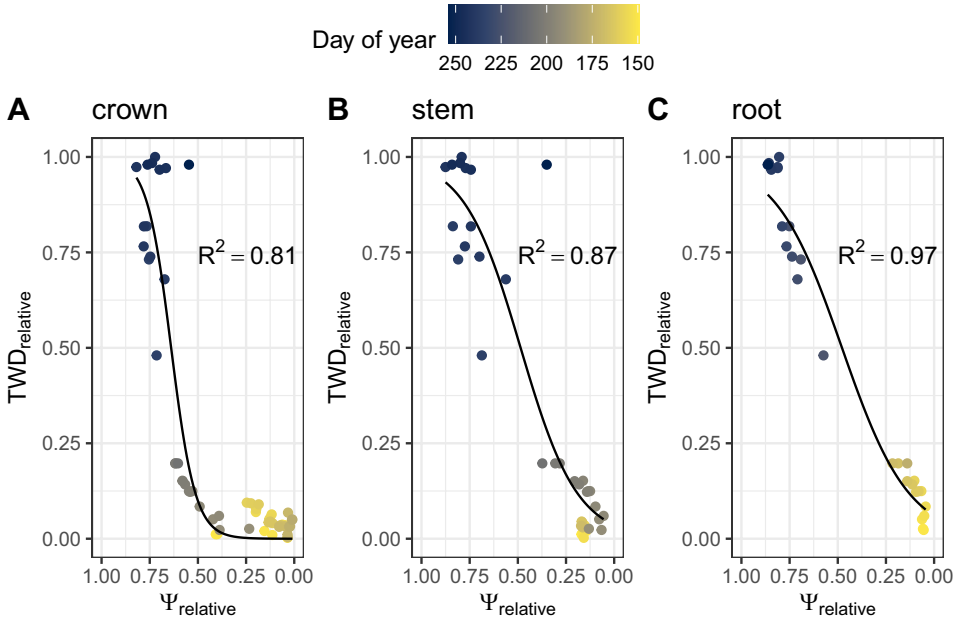


FIGURE 6 | Relationship between relative midday water potential and relative tree water deficit (TWD) exemplified for an ash tree during the vegetation period of 2024. The plots correspond to the tree compartment the microtensiometer was installed in (i.e., A = crown, B = stem, C = root). Dots are measured relative TWD and relative ψ_{stem}; the colour indicates the day of year in the vegetation period 2024; the black line represents the logistic model fit. R^2 is calculated from the quotient of the residual sum of squares and the total sum of squares.

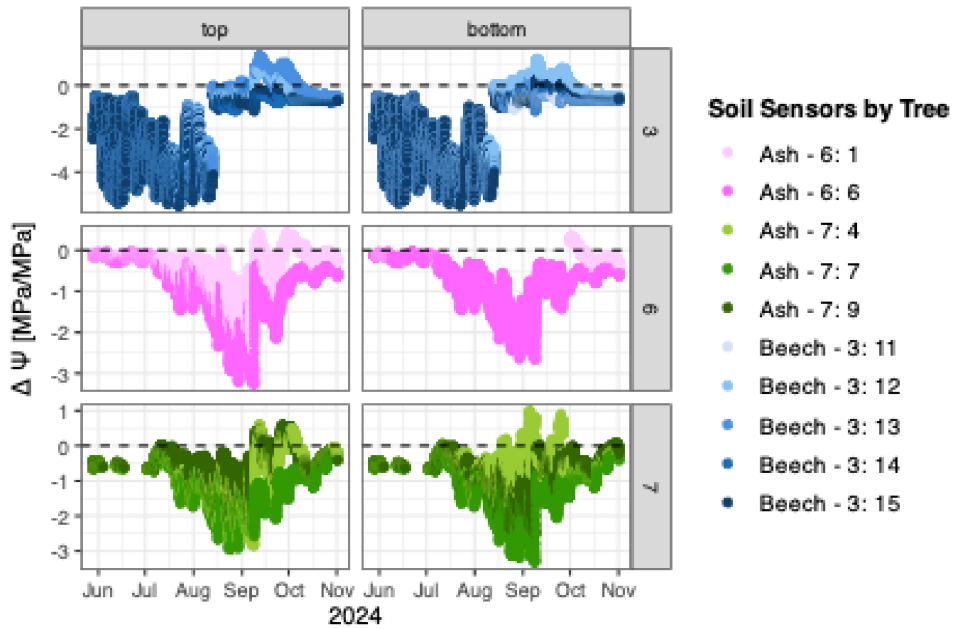


FIGURE 7 | Water potential gradients ($\Delta\psi$) between ψ_{stem} and ψ_{soil} for three trees (depicted as rows: 3-beech, 6-ash and 7-ash) for two measured soil depths (depicted as columns: top = −7.5 cm, bottom = −27.5 cm) at the Hainich plot in 2024. For each tree several matric potential sensors have been installed in the respective rhizosphere (at different distances within 2-m vicinity of the tree stem) and colours indicate which sensor is associated with which tree (e.g., pink coloured sensors 1 and 6 are associated with tree 6 ash). The black dashed horizontal line intercepts the *y*-axis at 0, values above that line indicate water uptake restrictions, while values below indicate the possibility for water uptake.

19360592, 2026, 3, Downloaded from https://onlinelibrary.wiley.com/doi/10.1002/eco.70197 by MPI 322 Chemical Ecology, Wiley Online Library on [30/03/2026]. See the Terms and Conditions (https://onlinelibrary.wiley.com/terms-and-conditions) on Wiley Online Library for rules of use; OA articles are governed by the applicable Creative Commons License

is physically possible from both the layers (i.e., −7.5 top and −27.5 cm bottom) and from all horizontal sensor positions associated with the respective rooting system until approximately mid-August. However, with the beginning of the short dry-down period in late August/beginning of September, the gradient becomes positive for most soil locations inside the rooting zone, and water uptake is no longer possible from those regions. Instead, water uptake was restricted to layers below 27.5 cm. There are some notable exceptions: Sensor 6 in the rooting zone of tree 6 (ash), and sensor 7 in the rooting zone of tree 7 (ash), remain potential RWU locations during the entire dry-down (Figure 7).

4 | Discussion

We assessed and proved the usability of a novel microtensiometer and extended the list of tree species it has been successfully tested on to hornbeam, beech and ash. We were able to monitor ψ_{stem} using the same sensors over two consecutive vegetation periods including re-installation after the winter period (2023/24).

4.1 | Microtensiometers Can Provide Accurate ψ_{stem} Measurements Depending on Correct Installation Procedures

Correctly installed microtensiometers delivered good agreements with ψ_{leaf} (Figure 2 and Figure 3) and realistic daily cycles (Figure 4). However, care should be taken when installing in ring-porous tree species (such as e.g. ash or oak), since it is crucial to instal the microtensiometers into the conducting xylem, which can be very narrow for ring-porous species (Zimmermann 1983). Generally, installing sensors in thick-barked species should be done carefully, and we recommend assessing bark depth prior to installation (e.g., using a bark gauge).

Water intrusion of the installation site was also a common issue that can be resolved when prevented by an umbrella-like roof made from e.g. silicone. However, if a sensor was flooded, it had to be re-installed. Therefore, we recommend adding the roof structure at first installation (see Magh and Paligi 2024 for details). The third most common issue we faced was related to signal transmission and cable length. Two solutions exist: either to use a digital converter with the analogue probe or shielded cables. The somewhat costly digital converter transfers the analogue signal to digital at the site of recording and cable extension is simple. More detailed descriptions and solutions are presented in Magh and Paligi (2024).

Direct comparison between ψ_{leaf} measured by the pressure chamber and ψ_{stem} measured by the microtensiometer showed good agreement for beech and hornbeam, as has been previously shown for pear trees (Blanco and Kalcsits 2021), apple trees (Blanco and Kalcsits 2024) and grapevines (Pagay 2022). However, contradictory to these studies, we found differences between early morning and midday water potential agreements between the methods, indicating that the change in offset (from the 1:1 line in Figure 2) is not constant. Put simply, it seems that the hydrostatic gradient is not the only process at work. The resulting shape of the relation is thus not linear but curved toward ψ_{midday} (Figure 2 and Table S2).

This shape could be related to changes in storage, which is fuller in the morning after nighttime rehydration of the stem and subsequently emptied daily throughout the day (Dobbs and Scott 1971; Meinzer et al. 2004). After the use of stored water for transpiration, the water transpired comes from the soil and must overcome a larger distance facing higher resistance than stored water (Cermak et al. 2007; Goldstein et al. 1998; Turcotte et al. 2011). The timing of these water usage patterns may vary between species and even among individual trees. Factors such as xylem vulnerability to embolism, hydraulic strategies and wood traits would contribute to these differences. For instance, a study examining nine dry forest tree species found significant interspecific variations in diurnal changes in embolism rates, which were linked to species-specific xylem vulnerability and hydraulic strategies (McCulloh and Meinzer 2015; Trifilò et al. 2015). This suggests that species like beech and hornbeam may exhibit different timings in their water storage depletion and replenishment cycles, reflecting their unique physiological adaptations. Exploring the relation between stem water storage, ψ_{leaf} and transpirational flux is a promising future application for microtensiometers that could be explored in the future on larger datasets.

4.2 | Species and Soil Matric Potential Explain Variations in ψ_{stem} During Nondrought Conditions

Our study identified that tree species identity and ψ_{soil} across upper and lower soil layers were the most important predictors of ψ_{stem} throughout the day at all three sites. Notably, species identity exhibited the highest predictive power during the early morning (peaking at 8:00) and evening (second peak at 20:00) (Figure 5a), periods characterized by lower transpiration demand. Concurrently, our model indicated an increased significance of ψ_{soil} in the upper soil layer between those times.

During these periods (i.e., early morning and evening/night) the primary physiological process is rehydration of internal water storage (Cermak et al. 2007), which is species specific. In the late afternoon, as transpiration decreases, trees begin to restore their water reserves and may also repair embolized xylem vessels (Zimmermann 1983; Trifilò et al. 2015; Klein et al. 2018). This replenishment process continues until transpiration resumes the following morning, as long as the gradient between the soil and the replenishment site remains (Klepper 1968). Consequently, the xylem tension within the stem reduces, a phenomenon corroborated by our data (Figure 4). Not surprisingly species identity was the most important driver explaining ψ_{stem}. The two diffuse-porous species (i.e., beech and hornbeam) differed strongly from the ring-porous species (ash), with ash retaining a more negative ψ_{stem} from evening through morning (Figure 4). This difference is likely related to variations in wood anatomy and the associated resistance of the xylem (Zimmermann 1983). While

19360592, 2026, 3, Downloaded from https://onlinelibrary.wiley.com/doi/10.1002/eco.70197 by MPI 322 Chemical Ecology, Wiley Online Library on [30/03/2026]. See the Terms and Conditions (https://onlinelibrary.wiley.com/terms-and-conditions) on Wiley Online Library for rules of use; OA articles are governed by the applicable Creative Commons License

diffuse-porous species generally exhibit lower hydraulic conductivity due to their smaller and more numerous vessels, ring-porous species—characterized by wider vessels—are more susceptible to embolism (Zimmermann 1983; Lösch 2003; von Allmen et al. 2015). This increased vulnerability can lead to higher flow resistance, requiring lower water potentials to sustain transpiration (Christman et al. 2012; Litvak et al. 2012). These interspecific differences are consistent with findings by Szatniewska et al. (2022), who reported contrasting water-use strategies between hornbeam and ash and related them to wood anatomy, species growth strategies and site characteristics. In particular, their observation of high transpiration rates in hornbeam aligns with our finding that hornbeam can substantially lower its water potential during periods of high transpirational demand (midday; Figure 4).

Soil water potentials were the second important predictors for ψ_{stem}. Although the exact depths depend on the measurement site (the upper ranging from 10 to 15 cm and the lower from 30- to 230-cm soil depth), they all have in common that the lower soil layer was moister (had a less negative ψ_{soil}) compared with the upper one. In all cases the upper ψ_{soil} featured the highest importance during the day (i.e., after 10:00 and before 18:00), while the lower ψ_{soil} showed the opposite pattern (i.e., peaking at 10:00 and regaining importance after 18:00) (Figure 5b). This pattern highlights the importance of accessing different soil water pools under varying transpirational demand and supports the concept of dynamic shifts in water uptake depth among tree species (Bertrand et al. 2014; Brinkmann et al. 2019; Szatniewska et al. 2022).

The same pattern has previously been proposed in a study investigating the causes of temporal and spatial shifts in water isotopic signatures in the stem xylem (De Deurwaerder et al. 2020). To explain observed diurnal variations, the authors suggest that the plant cannot avail water from drier (and in most cases this is the upper) soil layers during times of low transpirational demand because the potential gradient is too low. This has previously been shown to be true for woody species (Klepper 1968). Our data suggest that deeper roots are active in water replenishment during night (when stem water potentials are less negative) while more shallow roots were active during the day (when stem water potentials were more negative), which is in line with total water potentials being dependent on where water flow occurs (Hildebrandt et al. 2016). We demonstrate this pattern under moderately dry to normal moisture conditions during the summer of 2023 (according to the 12-month SPEI; Figure S5), likely in the absence of severe soil water stress. It is conceivable that these dynamics become more pronounced during prolonged drought, when soil water potential gradients steepen further. Under such conditions, the ability of individual trees to shift water uptake depth while maintaining functional access to biologically active upper soil layers is likely to depend strongly on species identity and site characteristics, as shown by Hackmann et al. (2025), Mrak et al. (2025) and Szatniewska et al. (2022). Longer time series would be required to fully capture these interactions and to assess the increasing role of atmospheric forcing during drought.

4.3 | Microtensiometers Provide Potential in Unravelling the Complex Challenges in Plant Hydraulics

We tested microtensiometers in two additional settings to further demonstrate its utility when investigating the relationship between TWD and canopy water potential (ψ_{canopy}) (Dietrich et al. 2018; Ziegler et al. 2024), as well as their potential as a tool for determining physiological constraints in RWU patterns (e.g., Magh et al. 2020; De Deurwaerder et al. 2020).

4.3.1 | Relation Between TWD and Plant Water Potential

In their original research, Dietrich et al. (2018) used TWD as a proxy for predicting canopy water potential, an approach that required extensive manual and destructive sampling of leaf water potentials. In contrast, by employing microtensiometers, we were able to continuously collect data from both the dendrometer and microtensiometer with minimal intervention. Our results confirm that the logistic relationship proposed between TWD and ψ_{canopy} also holds for $\psi_{root,}$ ψ_{stem} and ψ_{crown}, reinforcing the broader applicability of this method. With our findings we can show that the nonlinear relationship, which includes the decoupling of TWD and ψ at high and low ψ, which is correlating with ψ_{soil} of the upper layer. Dietrich et al. (2018) suggested that this decoupling at very low ψ was the result of cavitation of tracheids/vessels in the xylem with resulting loss in axial and radial conductance. We can show here that if that is the case, it is likely caused by the low ψ_{soil} in the upper soil layers (Figure 6).

This validation paves the way for more extensive studies across diverse species and forest ecosystems, allowing researchers to investigate tree responses to atmospheric and environmental conditions in a continuous and less labour-intensive way (Novick et al. 2022).

4.3.2 | Physical Constraints for RWU Determinations

Our results indicate that the gradients in water potential between the stem and the soil are not simply driven by depth but to a similar amount by spatial components within the root system (Figure 6), which has previously been demonstrated for soil solution chemistry (Koch and Matzner 1993), as well as for soil properties (Metzger et al. 2021), and soil moisture and therein estimated RWU (Demir et al. 2024). Hence, although soil heterogeneity is frequently discussed in soil science it is often overlooked in calculations of RWU depths and patterns—particularly when relying on methods such as stable isotope analysis (e.g., Dawson and Pate 1996; Brooks et al. 2010; Moreno-Gutiérrez et al. 2012; Barbeta and Peñuelas 2017; Brum et al. 2019).

Despite the known spatial variability in soil moisture and RWU, it remains common practice to instal a single soil pit and extrapolate its data across entire study plots. However, this approach can significantly misrepresent actual RWU dynamics—especially when methods like stable isotope analysis rely on such

19360592, 2026, 3, Downloaded from https://onlinelibrary.wiley.com/doi/10.1002/eco.70197 by MPI 322 Chemical Ecology, Wiley Online Library on [30/03/2026]. See the Terms and Conditions (https://onlinelibrary.wiley.com/terms-and-conditions) on Wiley Online Library for rules of use; OA articles are governed by the applicable Creative Commons License

simplified soil data. Our findings indicate that water uptake dynamics exhibit great spatial variability both horizontally and vertically, underscoring the importance of considering moisture content variations in both dimensions to achieve accurate RWU pattern estimates. This approach represents a simplification, as it assumes instantaneous equilibrium and neglects tree internal buffering and capacitance. Consequently, RWU estimates should be interpreted with caution; nevertheless, the method provides a rapid and practical indication of RWU during e.g. drying phases in the investigated forest.

This perspective aligns with studies emphasizing the significance of horizontal soil water potential heterogeneity in modelling crop water dynamics. For instance, Couvreur et al. (2014) demonstrated that neglecting horizontal heterogeneity within the root zone can lead to inaccuracies in hydrological models, particularly for crops with nonuniform lateral root distributions. Similarly, von Jeetze et al. (2020) found that microscale soil heterogeneity affects water flow and pressure distribution at the root–soil interface, influencing RWU rates and plant water stress recovery.

To address these challenges, we emphasize the potential of combining microtensiometers with a spatially extensive soil matric potential sensor network that fully captures the rooting zones of monitored trees. This setup enables a more accurate representation of physical constraints to water uptake across both vertical and horizontal axes, overcoming the oversimplifications inherent in single-point soil measurements.

5 | Conclusion

This study provides a glimpse into the broader potential of microtensiometers by demonstrating their potential to continuously monitor plant water status across multiple organs (root and stem) in important mature forest tree species. Our findings highlight microtensiometers as a promising, minimally invasive (compared with pressure chamber measurements) and low-cost method (compared with stem psychrometers, also in the long run to scholander pressure chamber) for directly measuring xylem water potential. However, careful sensor installation and routine maintenance are essential to ensure reliable and accurate data acquisition.

Beyond advancing plant hydraulics, our findings have direct relevance for ecohydrology and land surface modelling. By resolving continuous stem water potential dynamics and their dependence on both species identity and soil matric potential across multiple soil layers, this study provides empirical constraints for representing vegetation water stress in land surface models, where stem water potential remains poorly parameterized. The observed species-specific responses and the temporally shifting importance of upper versus deeper soil layers demonstrate that plant water status integrates both atmospheric demand and spatially heterogeneous soil water availability, even under nondrought conditions. Continuous microtensiometer measurements therefore offer a means to link soil drying and meteorological forcing with whole-tree water status in a mechanistic and temporally explicit way. From an applied perspective, real-time, in situ monitoring of tree water potential provides actionable information for forest and urban forestry practitioners, enabling improved assessment of drought responses, identification of vulnerable species or individuals, and more informed management decisions under increasing climatic variability.

Author Contributions

R.K.M., A.K., C.A., M.B., M.D., C.W. and A.H. acquired funding for instrumentation and setting up of the campaigns; R.K.M., S.S.P., S.H., M.D., M.B. and A.K. planned the campaigns; R.K.M., S.S.P., C.R. and S.H. performed the measurements and curated the data; R.K.M. and P.P. did the formal analyses; R.K.M. wrote the original draft; all authors reviewed and edited the manuscript.

Acknowledgements

The authors acknowledge the support with installation and/or data maintenance from the following people: **Hainich**: Laura Donfack Somenguem, Gökben Demir, Christina Hackmann, Björn Lüdecke, Constantin Funck, Tiana Hammer, David Römermann, Viktor Schreier, Frank Tiedemann, Jan Niklas Eiken and Anna-Lena Günther. **Apelern**: Bernard Luers, Ferdinand Exler, Marten Schmidt, David Dubbert. **Hartheim**: Fabio Scarpa, Stefan Seeger, Andreas Christen, Thomas Plapp, Dirk Redepenning. We further thank Felix Pohl for the SPEI Data. We acknowledge the help of Lars Dietrich for sharing his R-script to calculate the TWD. Finally, we thank the administration of the Hainich National Park for the opportunity to conduct research within the National Park. Open Access funding enabled and organized by Projekt DEAL.

Funding

This study is part of the Collaborative Research Centre AquaDiva of the Friedrich Schiller University Jena, funded by the Deutsche Forschungsgemeinschaft (DFG, German Research Foundation)—Project-ID 218627073—SFB 1076. SSP acknowledges financial support received from the German Research Foundation (DFG) through the Research Training Group 2300 (316045089/GRK2300). SH and CW acknowledge funding from the DFG SFB 1537 (ECOSENSE)—Project-ID 459819582. MB and MD acknowledge funding from the DFG under project numbers 501530203 and 538393318. AK and CA acknowledge support by Niedersächsisches Vorab (grant no. ZN 3679) and Ministry of Lower Saxony for Science and Culture (MWK) within the joint project 'Digital Forest', and the German Federal Ministry of Education and Research (BMBF; research infrastructure ICOS).

Conflicts of Interest

The authors declare no conflicts of interest.

Data Availability Statement

Data can be requested from RKM for the Hainich and ZALF Datasets, from SH for the Hartheim Dataset and from MD, CR and MB for the Apelern Dataset. R-Scripts are available upon request by RKM and Phython-Scripts from PP.

References

Barbeta, A., and J. Peñuelas. 2017. "Relative Contribution of Groundwater to Plant Transpiration Estimated With Stable Isotopes." *Scientific Reports* 7: 10580. https://doi.org/10.1038/s41598-017-09643-x.

Bertrand, G., J. Masini, N. Goldscheider, et al. 2014. "Determination of Spatiotemporal Variability of Tree Water Uptake Using Stable Isotopes (δ18O, δ2H) in an Alluvial System Supplied by a High-Altitude

19360592, 2026, 3, Downloaded from https://onlinelibrary.wiley.com/doi/10.1002/eco.70197 by MPI 322 Chemical Ecology, Wiley Online Library on [30/03/2026]. See the Terms and Conditions (https://onlinelibrary.wiley.com/terms-and-conditions) on Wiley Online Library for rules of use; OA articles are governed by the applicable Creative Commons License

Watershed, Pfyn Forest, Switzerland." *Ecohydrology* 7: 319–333. https://doi.org/10.1002/eco.1347.

Bhaskar, R., and D. d. Ackerly. 2006. "Ecological Relevance of Minimum Seasonal Water Potentials." *Physiologia Plantarum* 127: 353–359. https://doi.org/10.1111/j.1399-3054.2006.00718.x.

Blanco, V., and L. Kalcsits. 2021. "Microtensiometers Accurately Measure Stem Water Potential in Woody Perennials." *Plants* 10: 2780. https://doi.org/10.3390/plants10122780.

Blanco, V., and L. Kalcsits. 2024. "Relating Microtensiometer-Based Trunk Water Potential With Sap Flow, Canopy Temperature, and Trunk and Fruit Diameter Variations for Irrigated 'Honeycrisp' Apple." *Frontiers in Plant Science* 15: 1393028. https://doi.org/10.3389/fpls.2024.1393028.

Bourbia, I., and T. J. Brodribb. 2023. "A New Technique for Monitoring Plant Transpiration Under Field Conditions Using Leaf Optical Dendrometry." *Agricultural and Forest Meteorology* 331: 109328. https://doi.org/10.1016/j.agrformet.2023.109328.

Bourbia, I., C. Lucani, and T. J. Brodribb. 2022. "Constant Hydraulic Supply Enables Optical Monitoring of Transpiration in a Grass, a Herb, and a Conifer." *Journal of Experimental Botany* 73: 5625–5633. https://doi.org/10.1093/jxb/erac241.

Bourbia, I., C. Pritzkow, and T. J. Brodribb. 2021. "Herb and Conifer Roots Show Similar High Sensitivity to Water Deficit." *Plant Physiology* 186: 1908–1918. https://doi.org/10.1093/plphys/kiab207.

Brinkmann, N., W. Eugster, N. Buchmann, and A. Kahmen. 2019. "Species Specific Differences in Water Uptake Depth of Mature Temperate Trees Vary With Water Availability in the Soil." *Plant Biology* 21: 71–81. https://doi.org/10.1111/plb.12907.

Brodersen, C. R., A. B. Roddy, J. W. Wason, and A. J. McElrone. 2019. "Functional Status of Xylem Through Time." *Annual Review of Plant Biology* 70: 407–433. https://doi.org/10.1146/annurev-arplant-050718-100455.

Brooks, J. R., H. R. Barnard, R. Coulombe, and J. J. McDonnell. 2010. "Ecohydrologic Separation of Water Between Trees and Streams in a Mediterranean Climate." *Nature Geoscience* 3: 100–104. https://doi.org/10.1038/ngeo722.

Brum, M., M. A. Vadeboncoeur, V. Ivanov, et al. 2019. "Hydrological Niche Segregation Defines Forest Structure and Drought Tolerance Strategies in a Seasonal Amazon Forest." *Journal of Ecology* 107: 318–333. https://doi.org/10.1111/1365-2745.13022.

Buckley, T. N. 2005. "The Control of Stomata by Water Balance." *New Phytologist* 168: 275–292. https://doi.org/10.1111/j.1469-8137.2005.01543.x.

Buckley, T., and L. Sack. 2024. "Resolving Micro-Scale Water Potential Gradients Within Leaves." *Journal of Plant Hydraulics* 10: 1–1. https://doi.org/10.20870/jph.2024.1.

Campbell, G. S., and M. D. Campbell. 1974. "Evaluation of a Thermocouple Hygrometer for Measuring Leaf Water Potential in Situ." *Agronomy Journal* 66: 24–27. https://doi.org/10.2134/agronj1974.00021962006600010007x.

Cermak, J., J. Kucera, W. L. Bauerle, N. Phillips, and T. M. Hinckley. 2007. "Tree Water Storage and Its Diurnal Dynamics Related to Sap Flow and Changes in Stem Volume in Old-Growth Douglas-Fir Trees." *Tree Physiology* 27: 181–198. https://doi.org/10.1093/treephys/27.2.181.

Choat, B., T. J. Brodribb, C. R. Brodersen, R. A. Duursma, R. López, and B. E. Medlyn. 2018. "Triggers of Tree Mortality Under Drought." *Nature* 558: 531–539. https://doi.org/10.1038/s41586-018-0240-x.

Christen, A., F. Baab, S. Kolbe, T. Plapp, D. Redepenning, and D. Schindler. "ETC L2 Meteosens from Hartheim, 2019-12-31–2023-12-31." 2024.

Christen, A., F. Imbery, L. Jaeger, A. Kessler, H. Mayer, and D. Schindler. 2024. "Climate Data at Hartheim Forest Research Site (DE-Har) for the Reference Period 1991–2020 [L2] (1.0.0)." https://doi.org/10.5281/zenodo.14292825.

Christman, M. A., J. S. Sperry, and D. D. Smith. 2012. "Rare Pits, Large Vessels and Extreme Vulnerability to Cavitation in a Ring-Porous Tree Species." *New Phytologist* 193: 713–720. https://doi.org/10.1111/j.1469-8137.2011.03984.x.

Cochard, H., L. Coll, X. Le Roux, and T. Améglio. 2002. "Unraveling the Effects of Plant Hydraulics on Stomatal Closure During Water Stress in Walnut." *Plant Physiology* 128: 282–290.

Couvreur, V., J. Vanderborght, L. Beff, and M. Javaux. 2014. "Horizontal Soil Water Potential Heterogeneity: Simplifying Approaches for Crop Water Dynamics Models." *Hydrology and Earth System Sciences* 18: 1723–1743. https://doi.org/10.5194/hess-18-1723-2014.

Dawson, T. E. 1993. "Hydraulic Lift and Water Use by Plants: Implications for Water Balance, Performance and Plant-Plant Interactions." *Oecologia* 95: 565–574. https://doi.org/10.1007/BF00317442.

Dawson, T. E., and J. S. Pate. 1996. "Seasonal Water Uptake and Movement in Root Systems of Australian PhraeatophyUc Plants of Dimorphic Root Morphology: A Stable Isotope Investigation." *Oecologia* 107: 13–20.

De Deurwaerder, H. P. T., M. D. Visser, M. Detto, et al. 2020. "Causes and Consequences of Pronounced Variation in the Isotope Composition of Plant Xylem Water." *Biogeosciences* 17: 4853–4870. https://doi.org/10.5194/bg-17-4853-2020.

De Swaef, T., O. Pieters, S. Appeltans, et al. 2022. "On the Pivotal Role of Water Potential to Model Plant Physiological Processes." *In Silico Plants* 4: diab038. https://doi.org/10.1093/insilicoplants/diab038.

Demir, G., A. J. Guswa, J. Filipzik, J. C. Metzger, C. Römermann, and A. Hildebrandt. 2024. "Root Water Uptake Patterns Are Controlled by Tree Species Interactions and Soil Water Variability." *Hydrology and Earth System Sciences* 28: 1441–1461. https://doi.org/10.5194/hess-28-1441-2024.

Dietrich, L., R. Zweifel, and A. Kahmen. 2018. "Daily Stem Diameter Variations Can Predict the Canopy Water Status of Mature Temperate Trees." *Tree Physiology* 38: 941–952. https://doi.org/10.1093/treephys/tpy023.

Dixon, M. A., and M. T. Tyree. 1984. "A New Stem Hygrometer, Corrected for Temperature Gradients and Calibrated Against the Pressure Bomb." *Plant, Cell & Environment* 7: 693–697. https://doi.org/10.1111/1365-3040.ep11572454.

Dobbs, R. C., and D. R. M. Scott. 1971. "Distribution of Diurnal Fluctuations in Stem Circumference of Douglas-Fir." *Canadian Journal of Forest Research* 1: 80–83. https://doi.org/10.1139/x71-010.

Donfack, L. S., M. Mund, F. Koebsch, et al. 2026. "Linking Sap Flow and Tree Water Deficit in an Unmanaged, Mixed Beech Forest During the Summer Drought 2022." *Plant Biology*. https://doi.org/10.1111/plb.13754.

Doussan, C., A. Pierret, E. Garrigues, and L. Pagès. 2006. "Water Uptake by Plant Roots: II—Modelling of Water Transfer in the Soil Root-System With Explicit Account of Flow Within the Root System—Comparison With Experiments." *Plant and Soil* 283: 99–117. https://doi.org/10.1007/s11104-004-7904-z.

Ehlig, C. F. 1962. "Measurement of Energy Status of Water in Plants With a Thermocouple Psychrometer." *Plant Physiology* 37: 288–290. https://doi.org/10.1104/pp.37.3.288.

Epila, J., W. H. Maes, H. Verbeeck, J. Van Camp, J. B. L. Okullo, and K. Steppe. 2017. "Plant Measurements on African Tropical *Maesopsis eminii* Seedlings Contradict Pioneering Water Use Behaviour."

19360592, 2026, 3, Downloaded from https://onlinelibrary.wiley.com/doi/10.1002/eco.70197 by MPI 322 Chemical Ecology, Wiley Online Library on [30/03/2026]. See the Terms and Conditions (https://onlinelibrary.wiley.com/terms-and-conditions) on Wiley Online Library for rules of use; OA articles are governed by the applicable Creative Commons License

Environmental and Experimental Botany 135: 27–37. https://doi.org/10.1016/j.envexpbot.2016.12.006.

Evaristo, J., J. J. McDonnell, and J. Clemens. 2017. "Plant Source Water Apportionment Using Stable Isotopes: A Comparison of Simple Linear, Two-Compartment Mixing Model Approaches." *Hydrological Processes* 31: 3750–3758. https://doi.org/10.1002/hyp.11233.

FloraPulse: Resources. 2025. https://www.florapulse.com/resources, last access: 10 February 2025.

Garcia-Forner, N., C. Biel, R. Savé, and J. Martínez-Vilalta. 2017. "Isohydric Species Are Not Necessarily More Carbon Limited Than Anisohydric Species During Drought." *Tree Physiology* 37: 441–455. https://doi.org/10.1093/treephys/tpw109.

Gleason, S. M., J. J. Stewart, B. Allen, et al. 2024. "Development and Application of an Inexpensive Open-Source Dendrometer for Detecting Xylem Water Potential and Radial Stem Growth at High Spatial and Temporal Resolution." *AoB Plants* 16: plae009. https://doi.org/10.1093/aobpla/plae009.

Goffin, S., M. Aubinet, M. Maier, C. Plain, H. Schack-Kirchner, and B. Longdoz. 2014. "Characterization of the Soil CO_2 Production and Its Carbon Isotope Composition in Forest Soil Layers Using the Flux-Gradient Approach." *Agricultural and Forest Meteorology* 188: 45–57. https://doi.org/10.1016/j.agrformet.2013.11.005.

Goldstein, G., J. L. Andrade, F. C. Meinzer, et al. 1998. "Stem Water Storage and Diurnal Patterns of Water Use in Tropical Forest Canopy Trees." *Plant, Cell & Environment* 21: 397–406. https://doi.org/10.1046/j.1365-3040.1998.00273.x.

Guo, J. S., K. R. Hultine, G. W. Koch, H. Kropp, and K. Ogle. 2020. "Temporal Shifts in Iso/Anisohydry Revealed From Daily Observations of Plant Water Potential in a Dominant Desert Shrub." *New Phytologist* 225: 713–726. https://doi.org/10.1111/nph.16196.

Haberstroh, S., F. Scarpa, S. Seeger, A. Christen, and C. Werner. 2025. "Continuous Stem Water Potential Measurements of a Diffuse-Porous Tree Species Offer New Insights Into Tree Water Relations." *Ecohydrology* 18: e2761. https://doi.org/10.1002/eco.2761.

Haberstroh, S., C. Werner, M. Grün, et al. 2022. "Central European 2018 Hot Drought Shifts Scots Pine Forest to Its Tipping Point." *Plant Biology* 24: 1186–1197. https://doi.org/10.1111/plb.13455.

Hackmann, C. A., S. S. Paligi, M. Mund, et al. 2025. "Root Water Uptake Depth in Temperate Forest Trees: Species-Specific Patterns Shaped by Neighbourhood and Environment." *Plant Biology*. https://doi.org/10.1111/plb.70058.

Harris, C. R., K. J. Millman, S. J. van der Walt, et al. 2020. "Array Programming With NumPy." *Nature* 585: 357–362. https://doi.org/10.1038/s41586-020-2649-2.

Henzler, T., R. N. Waterhouse, A. J. Smyth, et al. 1999. "Diurnal Variations in Hydraulic Conductivity and Root Pressure Can Be Correlated With the Expression of Putative Aquaporins in the Roots of *Lotus japonicus*." *Planta* 210: 50–60. https://doi.org/10.1007/s004250050653.

Hildebrandt, A., A. Kleidon, and M. Bechmann. 2016. "A Thermodynamic Formulation of Root Water Uptake." *Hydrology and Earth System Sciences* 20: 3441–3454. https://doi.org/10.5194/hess-20-3441-2016.

Hillel, D. 2003. *Introduction to Environmental Soil Physics*. 1st ed. Elsevier.

Hochberg, U., F. E. Rockwell, N. M. Holbrook, and H. Cochard. 2018. "Iso/Anisohydry: A Plant–Environment Interaction Rather Than a Simple Hydraulic Trait." *Trends in Plant Science* 23: 112–120. https://doi.org/10.1016/j.tplants.2017.11.002.

Holst, J., R. Barnard, E. Brandes, N. Buchmann, A. Gessler, and L. Jaeger. 2008. "Impacts of Summer Water Limitation on the Carbon Balance of a Scots Pine Forest in the Southern Upper Rhine Plain." *Agricultural and Forest Meteorology* 148: 1815–1826. https://doi.org/10.1016/j.agrformet.2008.06.008.

Hunter, J. D. 2007. "Matplotlib: A 2D Graphics Environment." *Computing in Science & Engineering* 9: 90–95. https://doi.org/10.1109/MCSE.2007.55.

Javaux, M., T. Schröder, J. Vanderborght, and H. Vereecken. 2008. "Use of a Three-Dimensional Detailed Modeling Approach for Predicting Root Water Uptake." *Vadose Zone Journal* 7: 1079–1088. https://doi.org/10.2136/vzj2007.0115.

Klein, T., M. J. B. Zeppel, W. R. L. Anderegg, et al. 2018. "Xylem Embolism Refilling and Resilience Against Drought-Induced Mortality in Woody Plants: Processes and Trade-Offs." *Ecological Research* 33: 839–855. https://doi.org/10.1007/s11284-018-1588-y.

Klepper, B. 1968. "Diurnal Pattern of Water Potential in Woody Plants." *Plant Physiology* 43: 1931–1934.

Knohl, A., E.-D. Schulze, O. Kolle, and N. Buchmann. 2003. "Large Carbon Uptake by an Unmanaged 250-Year-Old Deciduous Forest in Central Germany." *Agricultural and Forest Meteorology* 118: 151–167. https://doi.org/10.1016/S0168-1923(03)00115-1.

Knohl, A., F. Tiedemann, A. Klosterhalfen, C. Markwitz, and L. Siebicke. "ETC L2 Meteosens From Hainich, 2018-12-31–2023-12-31." 2024.

Koch, A. S., and E. Matzner. 1993. "Heterogeneity of Soil and Soil Solution Chemistry Under Norway Spruce (*Picea abies* Karst.) and European Beech (*Fagus silvatica* L.) as Influenced by Distance From the Stem Basis." *Plant and Soil* 151: 227–237. https://doi.org/10.1007/BF00016288.

Lakso, A. N., S. Zhu, M. Santiago, K. Shackel, V. Volkov, and A. D. Stroock. 2022. "A Microtensiometer Sensor to Continuously Monitor Stem Water Potentials in Woody Plants—Design and Field Testing." *Acta Horticulturae* 1335: 317–324. https://doi.org/10.17660/ActaHortic.2022.1335.39.

Litvak, E., H. R. McCarthy, and D. E. Pataki. 2012. "Transpiration Sensitivity of Urban Trees in a Semi-Arid Climate Is Constrained by Xylem Vulnerability to Cavitation." *Tree Physiology* 32: 373–388. https://doi.org/10.1093/treephys/tps015.

Lösch, R. 2003. *Wasserhaushalt der Pflanzen*. 1st ed. Quelle und Meyer Verlag.

Magh, R. K., C. Eiferle, T. Burzlaff, M. Dannenmann, H. Rennenberg, and M. Dubbert. 2020. "Competition for Water Rather Than Facilitation in Mixed Beech-Fir Forests After Drying-Wetting Cycle." *Journal of Hydrology* 587: 124944. https://doi.org/10.1016/j.jhydrol.2020.124944.

Magh, R.-K., and S. S. Paligi. 2024. "In-Situ Xylem Water Potential Measurements Using Microtensiometers."

McCulloh, K. A., and F. C. Meinzer. 2015. "Further Evidence That Some Plants Can Lose and Regain Hydraulic Function Daily." *Tree Physiology* 35: 691–693. https://doi.org/10.1093/treephys/tpv066.

McKinney, W. 2010. "Data Structures for Statistical Computing in Python." in Proceedings of the 9th Python in Science Conference, 56–61. https://doi.org/10.25080/Majora-92bf1922-00a.

Meinzer, F. C. 1993. "Stomatal Control of Transpiration." *Trends in Ecology & Evolution* 8: 289–294. https://doi.org/10.1016/0169-5347(93)90257-P.

Meinzer, F. C., S. A. James, and G. Goldstein. 2004. "Dynamics of Transpiration, Sap Flow and Use of Stored Water in Tropical Forest Canopy Trees." *Tree Physiology* 24: 901–909. https://doi.org/10.1093/treephys/24.8.901.

Mencuccini, M., S. Manzoni, and B. Christoffersen. 2019. "Modelling Water Fluxes in Plants: From Tissues to Biosphere." *New Phytologist* 222: 1207–1222. https://doi.org/10.1111/nph.15681.

Metzger, J. C., J. Filipzik, B. Michalzik, and A. Hildebrandt. 2021. "Stemflow Infiltration Hotspots Create Soil Microsites Near Tree Stems

19360592, 2026, 3, Downloaded from https://onlinelibrary.wiley.com/doi/10.1002/eco.70197 by MPI 322 Chemical Ecology, Wiley Online Library on [30/03/2026]. See the Terms and Conditions (https://onlinelibrary.wiley.com/terms-and-conditions) on Wiley Online Library for rules of use; OA articles are governed by the applicable Creative Commons License

in an Unmanaged Mixed Beech Forest." *Frontiers in Forests and Global Change* 4: 701293.

Moreno-Gutiérrez, C., T. E. Dawson, E. Nicolás, and J. I. Querejeta. 2012. "Isotopes Reveal Contrasting Water Use Strategies Among Coexisting Plant Species in a Mediterranean Ecosystem." *New Phytologist* 196, no. 2: 489–496. https://doi.org/10.1111/j.1469-8137.2012.04276.x.

Mrak, K., C. A. Hackmann, S. S. Paligi, et al. 2025. "De-Coupled Water and Nitrogen Translocation From Subsoil to Canopy of Temperate Forest Trees." *Plant, Cell & Environment*. https://doi.org/10.1111/pce.70327.

Mund, M., M. Herbst, A. Knohl, et al. 2020. "It Is Not Just a 'Trade-Off': Indications for Sink- and Source-Limitation to Vegetative and Regenerative Growth in an Old-Growth Beech Forest." *New Phytologist* 226: 111–125. https://doi.org/10.1111/nph.16408.

Novick, K. A., D. L. Ficklin, D. Baldocchi, et al. 2022. "Confronting the Water Potential Information Gap." *Nature Geoscience* 15: 158–164. https://doi.org/10.1038/s41561-022-00909-2.

Ogle, K., R. L. Wolpert, and J. F. Reynolds. 2004. "Reconstructing Plant Root Area and Water Uptake Profiles." *Ecology* 85: 1967–1978. https://doi.org/10.1890/03-0346.

Pagay, V. 2022. "Evaluating a Novel Microtensiometer for Continuous Trunk Water Potential Measurements in Field-Grown Irrigated Grapevines." *Irrigation Science* 40: 45–54. https://doi.org/10.1007/s00271-021-00758-8.

Pagay, V., M. Santiago, D. A. Sessoms, et al. 2014. "A Microtensiometer Capable of Measuring Water Potentials Below −10 MPa." *Lab on a Chip* 14: 2806–2817. https://doi.org/10.1039/C4LC00342J.

Paligi, S. S., J. Lichter, M. Kotowska, et al. 2024. "Water Status Dynamics and Drought Tolerance of Juvenile European Beech, Douglas Fir and Norway Spruce Trees as Dependent on Neighborhood and Nitrogen Supply." *Tree Physiology* 44: tpae044. https://doi.org/10.1093/treephys/tpae044.

Pedregosa, F., G. Varoquaux, A. Gramfort, et al. 2011. "Scikit-Learn: Machine Learning in Python." *Journal of Machine Learning Research* 12: 2825–2830.

Philip, J. R. 1966. "Plant Water Relations: Some Physical Aspects." *Annual Review of Plant Physiology* 17: 245–268. https://doi.org/10.1146/annurev.pp.17.060166.001333.

R Core Team: _R. 2023. "A Language and Environment for Statistical Computing."

Richards, L. A., and G. Ogata. 1958. "Thermocouple for Vapor Pressure Measurement in Biological and Soil Systems at High Humidity." *Science* 128: 1089–1090. https://doi.org/10.1126/science.128.3331.1089.

Savage, M. J., H. H. Wiebe, and A. Cass. 1983. "In Situ Field Measurement of Leaf Water Potential Using Thermocouple Psychrometers." *Plant Physiology* 73: 609–613. https://doi.org/10.1104/pp.73.3.609.

Schenk, H. J., K. Mocko, J. M. Michaud, et al. 2020. "In Situ Measurement of Plant Hydraulic Conductance." *Acta Horticulturae* 169–178. https://doi.org/10.17660/ActaHortic.2020.1300.22.

Scholander, P. F. 1966. "The Role of Solvent Pressure in Osmotic Systems." *Proceedings of the National Academy of Sciences of the United States of America* 55: 1407–1414.

Sperry, J. S., U. G. Hacke, R. Oren, and J. P. Comstock. 2002. "Water Deficits and Hydraulic Limits to Leaf Water Supply." *Plant, Cell & Environment* 25: 251–263. https://doi.org/10.1046/j.0016-8025.2001.00799.x.

Szatniewska, J., I. Zavadilova, O. Nezval, et al. 2022. "Species-Specific Growth and Transpiration Response to Changing Environmental Conditions in Floodplain Forest." *Forest Ecology and Management* 516: 120248. https://doi.org/10.1016/j.foreco.2022.120248.

Tamrakar, R., M. B. Rayment, F. Moyano, M. Mund, and A. Knohl. 2018. "Implications of Structural Diversity for Seasonal and Annual Carbon Dioxide Fluxes in Two Temperate Deciduous Forests." *Agricultural and Forest Meteorology* 263: 465–476. https://doi.org/10.1016/j.agrformet.2018.08.027.

Torres-Ruiz, J. M., H. Cochard, S. Delzon, et al. 2024. "Plant Hydraulics at the Heart of Plant, Crops and Ecosystem Functions in the Face of Climate Change." *New Phytologist* 241: 984–999. https://doi.org/10.1111/nph.19463.

Trifilò, P., A. Nardini, M. A. Lo Gullo, P. M. Barbera, T. Savi, and F. Raimondo. 2015. "Diurnal Changes in Embolism Rate in Nine Dry Forest Trees: Relationships With Species-Specific Xylem Vulnerability, Hydraulic Strategy and Wood Traits." *Tree Physiology* 35: 694–705. https://doi.org/10.1093/treephys/tpv049.

Turcotte, A., S. Rossi, A. Deslauriers, C. Krause, and H. Morin. 2011. "Dynamics of Depletion and Replenishment of Water Storage in Stem and Roots of Black Spruce Measured by Dendrometers." *Frontiers in Plant Science* 2: 21. https://doi.org/10.3389/fpls.2011.00021.

Van Rossum, G., and F. L. Drake. 2009. *Python 3 Reference Manual*. CreateSpace.

Volaire, F. 2018. "A Unified Framework of Plant Adaptive Strategies to Drought: Crossing Scales and Disciplines." *Global Change Biology* 24: 2929–2938. https://doi.org/10.1111/gcb.14062.

von Allmen, E. I., J. S. Sperry, and S. E. Bush. 2015. "Contrasting Whole-Tree Water Use, Hydraulics, and Growth in a Co-Dominant Diffuse-Porous vs. Ring-Porous Species Pair." *Trees* 29: 717–728. https://doi.org/10.1007/s00468-014-1149-0.

von Jeetze, P. J., M. Zarebanadkouki, and A. Carminati. 2020. "Spatial Heterogeneity Enables Higher Root Water Uptake in Dry Soil but Protracts Water Stress After Transpiration Decline: A Numerical Study." *Water Resources Research* 56: e2019WR025501. https://doi.org/10.1029/2019WR025501.

Walthert, L., and P. Schleppi. 2018. "Equations to Compensate for the Temperature Effect on Readings From Dielectric *Decagon MPS-2* and *MPS-6* Water Potential Sensors in Soils." *Journal of Plant Nutrition and Soil Science* 181: 749–759. https://doi.org/10.1002/jpln.201700620.

Wickham, H., M. Averick, J. Bryan, et al. 2019. "Welcome to the Tidyverse." *Journal of Open Source Software* 4, no. 43: 1686. https://doi.org/10.21105/joss.01686.

Wood, S. N. 2011. "Fast Stable Restricted Maximum Likelihood and Marginal Likelihood Estimation of Semiparametric Generalized Linear Models." *Journal of the Royal Statistical Society Series B: Statistical Methodology* 73: 3–36. https://doi.org/10.1111/j.1467-9868.2010.00749.x.

Ziegler, Y., R. Grote, F. Alongi, T. Knüver, and N. K. Ruehr. 2024. "Capturing Drought Stress Signals: The Potential of Dendrometers for Monitoring Tree Water Status." *Tree Physiology* 44: tpae140. https://doi.org/10.1093/treephys/tpae140.

Zimmermann, M. H. 1983. *Xylem Structure and the Ascent of Sap*. Springer-Verlag.

Supporting Information

Additional supporting information can be found online in the Supporting Information section. **Table S1:** Distances (m) between the middle of the main stem of the individual trees and the installed soil sensor pairs at the Hainich plot. **Table S2:** Mean differences and standard deviations between ψleaf and ψstem separated by species over the course of a day for the ZALF dataset. Means are calculated from the 3-day observational course (n = 3), the same as standard deviations. **Figure S1:** Standardized Precipitation-Evapotranspiration Index (SPEI) for the Hainich field site during the measured months of the vegetation period 2024. Colour coding represents the SPEI-classes and lines represent the time periods (dashed line = 12 months SPEI, solid line = 3 months SPEI). 12 months better represents the entire time frame

19360592, 2026, 3, Downloaded from https://onlinelibrary.wiley.com/doi/10.1002/eco.70197 by MPI 322 Chemical Ecology, Wiley Online Library on [30/03/2026]. See the Terms and Conditions (https://onlinelibrary.wiley.com/terms-and-conditions) on Wiley Online Library for rules of use; OA articles are governed by the applicable Creative Commons License

e.g. for a hydrological year (here from the last vegetation period till now) and 3 month the shorter time frame (e.g., growth conditions during the vegetation period). **Figure S2:** R2 of test datasets for the hourly random forest regressions. **Figure S3:** SHAP (SHapley Additive exPlanations) waterfall plots for predicting ψstem at (a) 10:00 and (b) 16:00 o'clock. The plots illustrate the additive contribution of each environmental and biological feature to the final model prediction. E[f(X)] is the expected value across the entire dataset and f(x) is the specific prediction for the given time step. Red bars indicate positive SHAP values, where a feature increases the prediction (here, ψstem) relative to the mean, while blue bars indicate negative SHAP values, where a feature decreases it. **Figure S4:** Standardized Precipitation-Evapotranspiration Index (SPEI) for three months-interval during the measurement period in 2023 (i.e., with respect to the previous three months) at the three field sites (Apelern = solid line, Hainich = short-dashed line, Hartheim = long-dashed line). Colours represent the categorization of dry- and wetness severity. **Figure S5:** Standardized Precipitation-Evapotranspiration Index (SPEI) for 12 months-interval during the measurement period in 2023 (i.e., with respect to the previous 12 months) at the three field sites (Apelern = solid line, Hainich = short-dashed line, Hartheim = long-dashed line). Colours represent the categorization of dry- and wetness severity.

19360592, 2026, 3, Downloaded from https://onlinelibrary.wiley.com/doi/10.1002/eco.70197 by MPI 322 Chemical Ecology, Wiley Online Library on [30/03/2026]. See the Terms and Conditions (https://onlinelibrary.wiley.com/terms-and-conditions) on Wiley Online Library for rules of use; OA articles are governed by the applicable Creative Commons License